J. Min. Metall. Sect. B-Metall. 53 (3) B (2017) 333 - 340

Journal of Mining and Metallurgy, Section B: Metallurgy

ELECTROCHEMICAL CORROSION OF Al-Pd ALLOYS IN HCl AND NaOH SOLUTIONS

M. Palcut [a], L. Ďuriška [a], M. Špoták [a], M. Vrbovský [a], Ž. Gerhátová [a], I. Černičková [a], J. Janovec [b, *]

[a] Slovak University of Technology in Bratislava, Faculty of Materials Science and Technology in Trnava, Trnava, Slovakia

[b] Slovak University of Technology in Bratislava, University Science Park, Bratislava, Slovakia

(Received 25 April 2017; accepted 04 September 2017)

Abstract

The corrosion performance of as-solidified Al–Pd alloys in HCl and NaOH aqueous solutions is investigated in this work. Four different alloys ($Al_{88}Pd_{12}$, $Al_{77}Pd_{23}$, $Al_{72}Pd_{28}$ and $Al_{67}Pd_{33}$, element concentrations are given in at.%) were prepared from high purity Al and Pd lumps by arc–melting in Ar. Subsequently, the alloy microstructure and phase occurrence were investigated by a combination of scanning electron microscopy and room-temperature powder X–ray diffraction. The as-solidified Al–Pd alloys were found to consist of several single-phase microstructure constituents with various structures and chemical compositions, including structurally complex intermetallic phases. The polished surfaces of the Al–Pd alloys were subjected to electrochemical polarization in aqueous HCl and NaOH solutions (0.01 mol.dm^{-3}) at 21±2°C. The corrosion experiments were conducted in a standard 3–electrode cell controlled by potentiostat. The corrosion potentials and corrosion current densities were determined by Tafel extrapolation of the experimental polarization curves. Phase dissolution has been observed on the alloy surfaces and some of the phases were preferentially corroded. The effects of the alloy microstructure and the phase occurrence are evaluated. The local nobility of individual intermetallic compounds is discussed. Finally, the conclusions for the alloys corrosion performance in acidic and basic solutions are provided.

Keywords*: *Aluminium; Palladium; Complex metallic alloys; Corrosion; Alloy dissolution

1. Introduction

Binary Al–Pd alloys with compositions close to 27 at.% Pd belong to the complex metallic alloy (CMA) family. The CMAs are predominantly composed of structurally complex intermetallic phases of either crystalline or quasicrystalline nature [1]. The former type of phases consists of giant unit cells comprising hundreds or even thousands of atoms. In the latter type of phases, atoms are arranged non-periodically. Because of their complex crystal structure, the structurally complex intermetallic phases exhibit markedly different physical properties from those observed in traditional alloys [1]. Al-based CMAs have been utilized as scratch-resistant coatings [2]. Furthermore, possible applications of these materials in catalysis [3], hydrogen generation [4] and metal-matrix composites [5, 6] have been reported.

The Al-rich part of the Al–Pd phase diagram, proposed by Grushko [7] and reflecting partially the recent findings of Ďuriška et al. [8], is presented in Fig. 1. In Al–Pd alloys, the following phases have been identified [7]: (Al), λ-Al_4Pd, γ-$Al_{21}Pd_8$, ε_6 and ε_{28} (both ~Al_3Pd), δ-Al_3Pd_2, β-AlPd, β'-AlPd, μ-AlPd, υ-Al_3Pd_5, ρ-$AlPd_2$, τ-Al_2Pd_5, and (Pd). The metallographically non-distinguishable phases ε_6 and ε_{28} [8] are quasicrystalline approximants of orthorhombic structure, both exhibiting giant unit cells [9]. In this work, they are jointly denoted as ε_n. In the Al–Pd alloy system, ε_n is formed below about 790°C. It has, for instance, a low thermal conductivity combined with a moderate electrical resistivity [9]. Some of structurally complex intermetallic phases have a rich variety of different adsorption sites [10]; as such, they are interesting for catalysis [11-13].

Studies dealing with chemical properties and corrosion behaviour of CMAs are limited. Only few investigations have been reported so far and these include corrosion studies of Al–Co, Al–Cu–Fe, Al–Cr–Fe and Al–Cu–Fe–Cr CMAs in various electrolytes [14-23]. The electrochemical behaviour of rapidly solidified Al–Pd alloys has been studied in a NaCl aqueous solution only (1 mol.dm^{-3} [24]). A selective dissolution of Al (de-alloying) from

Dedicated to the memory of Professor Dragana Živković

* *Corresponding author: jozef.janovec@stuba.sk*

DOI:10.2298/JMMB170425015P

intermetallic phases in these alloys has been found. Electrochemical de-alloying is a phenomenon primarily originating from corrosion [25]. It has attracted much attention in recent years as it has been found to be efficient in creating nanoporous metal networks with a three-dimensional bi-continuous interpenetrating ligament-channel structure at the nanometer scale [26, 27]. Interactions between coexisting phases play an important role during de-alloying of a double-phase alloy. These interactions are, in principle, controlled by the diffusivity of the noble element (Pd), the curvature-dependent undercritical potential dissolution, and chemical reaction between the noble element and the chlorine ion [24].

To the best of our knowledge, the corrosion behaviour of Al–Pd complex metallic alloys in HCl and NaOH solutions has not been investigated yet. In industrial applications, the materials are often exposed to harsh environments including saline solutions and/or acid rains. The corrosion resistance of Al and its alloys in alkaline as well as acidic and saline environments is often very low due to protective oxide scale dissolution [28, 29]. Therefore, the electrochemical corrosion behaviour of Al–Pd alloys in HCl and NaOH electrolytes (0.01 mol dm^{-3}) has been studied in the present work through the potentiodynamic polarization. Surface morphology and phase compositional analyses were also conducted to provide the interpretation of the obtained polarization behaviour.

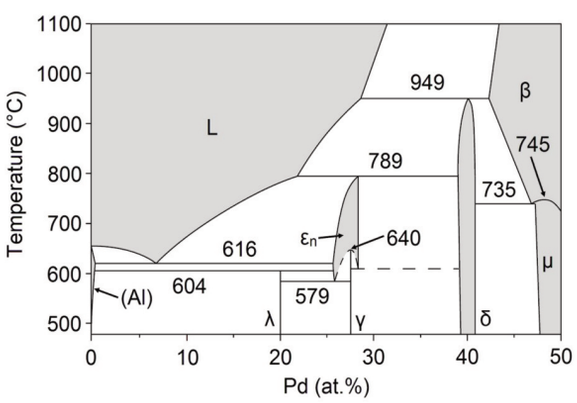

Figure 1. *Al–Pd phase diagram [7, 8]*

2. Material and methods

Four alloys, $Al_{88}Pd_{12}$, $Al_{77}Pd_{23}$, $Al_{72}Pd_{28}$ and $Al_{67}Pd_{33}$ (element concentrations are given in at.%) were investigated in the present work. The alloys nominal compositions were chosen to stay close to the ε_n (~Al_3Pd) chemical composition. The experimental Al-Pd alloys were prepared by arc melting of high purity (99.95 wt.%) Al and Pd lumps under argon atmosphere. The melt homogeneity was improved by repeated re-melting. A rapid solidification of the alloys was done by quenching the melted drops on a water-cooled Cu mould.

After solidification, the samples were mounted in epoxy resin, ground with SiC papers of various granularities and polished with diamond suspension down to 1 μm surface roughness. The polished sample surfaces were subjected to an electrochemical testing in a standard three electrode cell at 21±2°C. The Ag/AgCl electrode suspended in a saturated KCl solution (saturated silver chloride electrode, SSCE) was used as the reference electrode. A platinum sheet was used as the counter electrode. The corrosion experiments were carried out in aqueous HCl and NaOH solutions (0.01 mol dm^{-3}). The solutions were prepared by dissolving the weighted amount of HCl and NaOH respectively in de-ionized water. The electrochemical experiments were controlled by a PGU 10 V-1A-IMP-S potentiostat /galvanostat from Jaissle Electronic Ltd. (Waiblingen, Germany). The open circuit potential (OCP) of the alloys was measured during first 30 min of the sample immersion in the electrolyte. After stabilization, the electrochemical polarization experiments were carried out using a sweeping rate of 1 mV/s. The potential range for each measurement was chosen according to the OCP of the alloy and covered a minimum of 500 mV around the OCP on both anodic and cathodic sides. This corresponded to potentials between -1700 and -300 mV (SSCE) for NaOH and -1300 and +400 mV (SSCE) for HCl solutions. The resulting polarization curves were analyzed by the Tafel extrapolation.

The alloy microstructures before the electrochemical testing were studied by a scanning electron microscope (SEM) JEOL JSM-7600F, using the back-scattered electron imaging at 20 kV. For the energy-dispersive X-ray spectroscopy (EDX), an Oxford Instruments X-max 50 spectrometer working with INCA software was used. To obtain mean values of metal concentrations, at least ten measurements per constituent/phase were done. Similarly, average volume fractions were determined from a minimum of ten measurements. The microstructures of corroded samples were documented by a light microscope NEOPHOT 32. The powder X-ray diffraction (XRD) was carried out by using a Panalytical Empyrean PIXCel 3D diffractometer with Bragg-Brentano geometry, working with an iron filtered CoKα1,2 radiation. The X-ray scattering was performed for 2θ angle between 20° and 60°. The step size was 0.0131°, and the exposure time was 98 seconds per step.

Two sets of samples were investigated in this work, corresponding to as-solidified (i.e. original) and corroded (i.e. after the electrochemical testing) conditions.

3. Results and Discussion

All the as-solidified microstructures, given in Fig. 2, were observed to consist of two microstructure constituents. Each of the constituents was identified as a single-phase area. The alloys $Al_{88}Pd_{12}$ and $Al_{77}Pd_{23}$ were found to comprise (Al) and ε_n (ε_6+ε_{28}). In the alloys $Al_{72}Pd_{28}$ and $Al_{67}Pd_{33}$, ε_n (ε_6+ε_{28}) and δ were identified respectively. To perform the phase-to-constituent assignment, metal compositions available in Table 1 were compared with both SEM-micrographs (Fig. 2) and XRD-patterns (Fig. 3). This procedure led to the unambiguous structure characterization of the as-solidified alloys. In Fig. 3, only two characteristic XRD patterns are documented, each for one pair of the as-solidified alloys, showing the same phase constitution (see above). As the back-scattered electron imaging was used in the SEM observation, the constituents/phases exhibiting brighter appearance were revealed to contain more Pd (Fig. 2). Alloys with the same phase constitution were found to differ from one another in phase volume fractions (Table 1). On the other hand, each phase showed only negligible changes in metal composition across the set of investigated alloys (Table 1). The phase-to-constituent assignment is presented in Fig. 2 for each the as-solidified alloy.

The corrosion performance of the as-solidified Al–Pd alloys has been studied by potentiodynamic polarization in aqueous HCl and NaOH solutions at 21±2°C. At the beginning a steady-state open circuit potential (free corrosion potential) has been measured for 30 min of sample immersion in the electrolyte. The variation of the OCP with time is illustrated in Figs. 4 and 5. The measurement of Al is also included for comparison. The OCP values after 30 minutes of sample immersion increase in the following order in both electrolytes:

$$Al < Al_{88}Pd_{12} \sim Al_{77}Pd_{23} < Al_{72}Pd_{28} \sim Al_{67}Pd_{33} \quad ..(1)$$

The OCPs of the alloys increase with increasing Pd concentration in both solutions. This observation is in accordance with expectations since Pd has a higher standard electrochemical potential compared to Al [30]. The OCPs of the alloys $Al_{72}Pd_{28}$ and $Al_{67}Pd_{33}$ were nearly identical and significantly higher compared to alloys $Al_{88}Pd_{12}$ and $Al_{77}Pd_{23}$ (Figs. 4 and 5). Since these two alloy groups are composed of different phases (Table 1), the OCPs are not only determined by the bulk chemical composition, but are also influenced by a combination of structural factors including phase occurrence.

The OCP of aluminium was stable at the beginning of measurement; however, it eventually began to decrease in HCl solution as a result of corrosion. The OCPs of the Al–Pd alloys, on the other hand, were found to be relatively stable over time. Small potential oscillations have been found for alloys $Al_{72}Pd_{28}$ and $Al_{67}Pd_{33}$ respectively. Similar oscillations have been observed for alloys $Al_{70}Pd_{30}$ and $Al_{77}Pd_{23}$

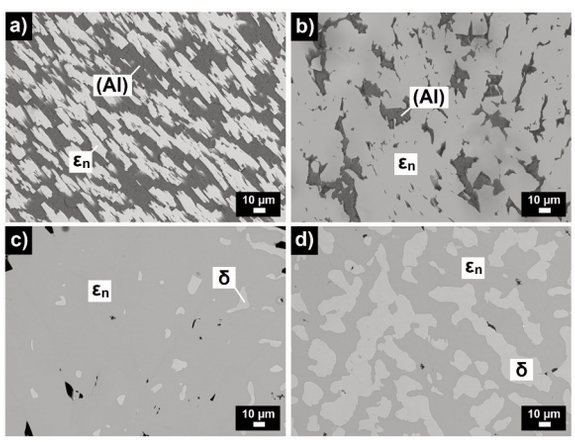

Figure 2. *Microstructures of as-solidified Al–Pd alloys: a) $Al_{88}Pd_{12}$, b) $Al_{77}Pd_{23}$, c) $Al_{72}Pd_{28}$, d) $Al_{67}Pd_{33}$. Microstructure constituents documented by SEM are assigned to phases identified by XRD.*

Table 1. *Volume fractions and metal compositions of phases/constituents identified in as-solidified Al–Pd alloys before electrochemical testing. For phase-to-constituent assignment see Fig. 2.*

Alloy denotation	Bulk metal composition (EDX/SEM) / at.% Pd	Phases identified (XRD)	Volume fraction of phase (SEM) / %	Phase metal composition (EDX/SEM) / at.%	
				Al	Pd
$Al_{88}Pd_{12}$	12.2±0.2	ε_n	48.1±0.1	73.6±0.1	26.4±0.1
		(Al)	51.9±0.1	99.7±0.1	0.3±0.1
$Al_{77}Pd_{23}$	23.2±0.4	ε_n	86.4±0.4	73.2±0.3	26.8±0.3
		(Al)	13.6±0.4	99.4±0.4	0.6±0.4
$Al_{72}Pd_{28}$	27.8±0.3	ε_n	97.7±0.3	72.5±0.1	27.5±0.1
		δ	2.3±0.3	59.1±0.2	40.9±0.2
$Al_{67}Pd_{33}$	33.4±0.3	ε_n	58.7±0.2	72.3±0.2	27.7±0.2
		δ	41.3±0.2	58.9±0.1	41.1±0.1

studied in NaCl solution previously [24]. These oscillations indicate that the Cl^{-1} present in the electrolyte probably interacts with the alloy phases and this interaction influences the open circuit potential.

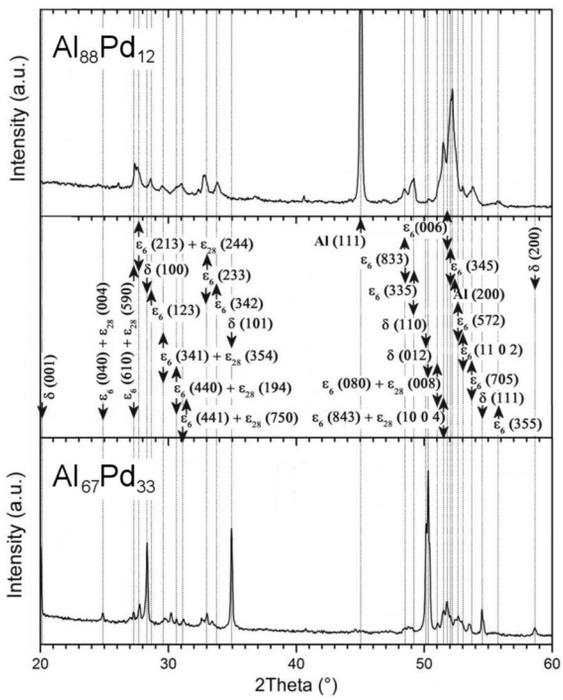

Figure 3. *XRD-patterns of alloys $Al_{88}Pd_{12}$ (upper) and $Al_{67}Pd_{33}$ (lower) linked with dotted lines corresponding to angular peak positions (2Theta). In the intermediate window, diffracting planes of particular phases are specified and assigned to peaks occurring in both XRD-patterns. Arrows with upwards/downwards oriented tips show the classification of corresponding diffracting plane to upper/lower patterns, respectively.*

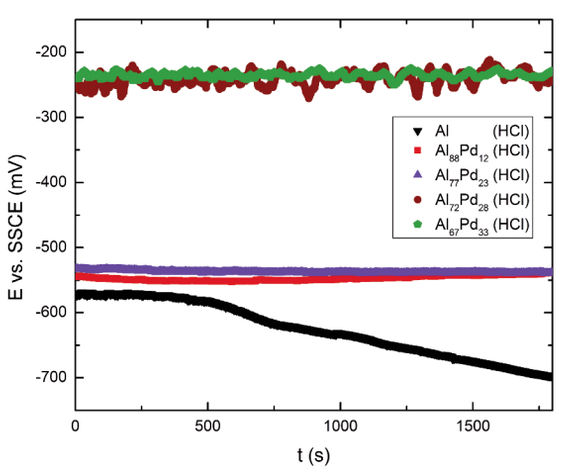

Figure 4. *Open circuit potentials of as-solidified Al–Pd alloys and Al in 0.01 M HCl as a function of time.*

The OCP values of the alloys measured in 0.01 M NaOH solution are considerably smaller compared to HCl (Tables 2 and 3). This observation shows a higher susceptibility towards corrosion in alkaline environments. This behaviour is in agreement with equilibrium E-pH diagram of Al. In this diagram, lower potentials of Al in equilibrium with ionic Al species in solution are found in alkaline environments [31]. In 0.01 M NaOH, the OCPs of alloys $Al_{77}Pd_{23}$, $Al_{72}Pd_{28}$ and $Al_{67}Pd_{33}$ have been found to slightly increase with time (Fig. 5). For the $Al_{88}Pd_{12}$ alloy and

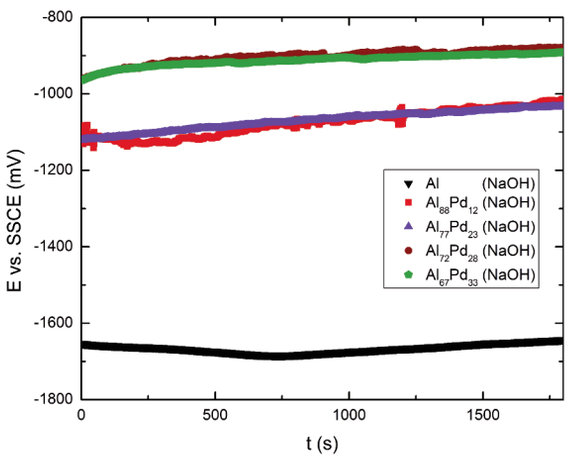

Figure 5. *Open circuit potentials of as-solidified Al–Pd alloys and Al in 0.01 M NaOH as a function of time.*

Table 2. *Electrochemical parameters of as-solidified Al–Pd alloys and Al after corrosion in 0.01 M HCl at 21±2°C.*

Alloy / Element	OCP / mV vs. SSCE	E_{corr} / mV vs. SSCE	i_{corr} / A m^{-2}
Al	-700	-768	0.1
$Al_{88}Pd_{12}$	-539	-478	0.26
$Al_{77}Pd_{23}$	-539	-450	0.27
$Al_{72}Pd_{28}$	-243	-253	0.03
$Al_{67}Pd_{33}$	-232	-200	0.17

Table 3*. Electrochemical parameters of as-solidified Al–Pd alloys and Al after corrosion in 0.01 M NaOH at 21±2°C.*

Alloy / Element	OCP / mV vs. SSCE	E_{corr} / mV vs. SSCE	i_{corr} / A m^{-2}
Al	-1657	-1458	4.51
$Al_{88}Pd_{12}$	-1019	-986	0.42
$Al_{77}Pd_{23}$	-1033	-1018	0.25
$Al_{72}Pd_{28}$	-879	-895	0.25
$Al_{67}Pd_{33}$	-892	-870	0.34

Al itself, an initial decrease of the OCP has been found which was, however, later followed by an increase of the OCP over time. This behaviour indicates a possible passivation of these materials in 0.01 M NaOH solution.

A further insight into corrosion behaviour of the Al–Pd alloys could be obtained by investigating the polarization behaviour. The polarization curves of the alloys in 0.01 M HCl are presented in Fig. 6. For alloys $Al_{88}Pd_{12}$, $Al_{77}Pd_{23}$ and $Al_{72}Pd_{28}$, a steep increase in the anodic current density has been found at potentials higher than corrosion potential. For the $Al_{67}Pd_{33}$ alloy, a small current-limiting stage could be distinguished. This transient stage has been followed by an increase of the current density at potentials above -100 mV (SSCE). This behaviour is similar to that of the Al corrosion behaviour (Fig. 6).

The polarization curves of Al and Al–Pd alloys in 0.01 M NaOH solution are presented in Fig 7. For Al–Pd alloys, a steady-state current density has been reached at potentials higher than the corrosion potential. For Al, a decrease of the current density has been found after an initial corrosion stage. This observation is indicative of passivation behaviour.

The polarization curves have been further analysed by the Tafel extrapolation [27] since the cathodic and anodic curves of most of the alloys had well-defined linear regions, extending over at least a decade of current. For the $Al_{67}Pd_{33}$ alloy and Al itself only cathodic curves were used since the anodic curves were significantly affected by immediate passivation (Figs. 6 and 7). The electrochemical parameters obtained from the curves are collected in Tables 2 and 3. The corrosion potentials obtained by sample polarization are close to the OCP values. The corrosion parameters vary with both the electrolyte and alloy bulk composition. Higher corrosion currents and lower corrosion potentials are found for 0.01 M NaOH solution. This observation indicates that Al–Pd alloys are more susceptible to general (uniform) corrosion in basic solutions compared to HCl. This result is in accordance with Al corrosion behaviour (Figs. 6 and 7).

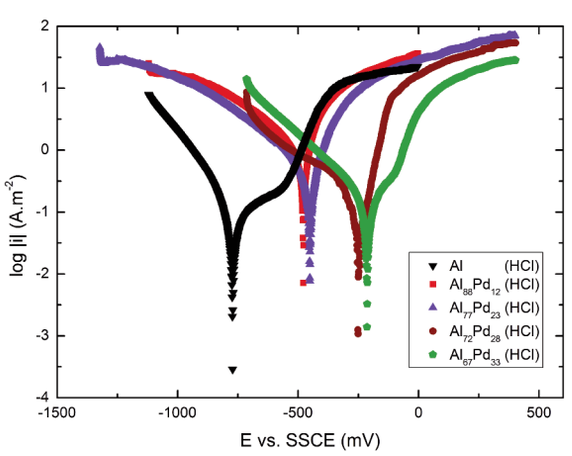

Figure 6. *Polarization curves of as-solidified Al–Pd alloys and Al in 0.01 M HCl.*

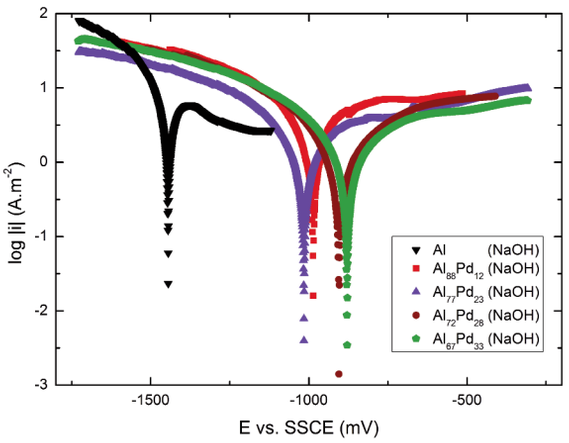

Figure 7. *Polarization curves of as-solidified Al–Pd alloys and Al in 0.01 M NaOH.*

More information about the specific corrosion attack of different intermetallic phases has been obtained by investigating the alloy microstructure after electrode polarization. Figs. 8 and 9 present the corroded microstructures after the electrochemical testing. In 0.01 M HCl aqueous solution, a preferential dissolution of (Al) in alloys $Al_{88}Pd_{12}$ and $Al_{77}Pd_{23}$ has been found (Figs. 8a and 8b). In the $Al_{72}Pd_{28}$ and $Al_{67}Pd_{33}$ alloys, a preferential corrosion attack of ε_n (Al_3Pd) has been observed (Fig. 8c and 8d). The corrosion attack of ε_n has resulted in a porous, channel-like framework (Fig. 8c). The inter-penetrating channels are probably a result of selective dissolution of Al from this phase (de-alloying).

In NaOH solution, a preferential dissolution of (Al) in alloys $Al_{88}Pd_{12}$ and $Al_{77}Pd_{23}$ has been found (Figs. 9a and 9b). For the $Al_{72}Pd_{28}$ and $Al_{67}Pd_{33}$ alloys,

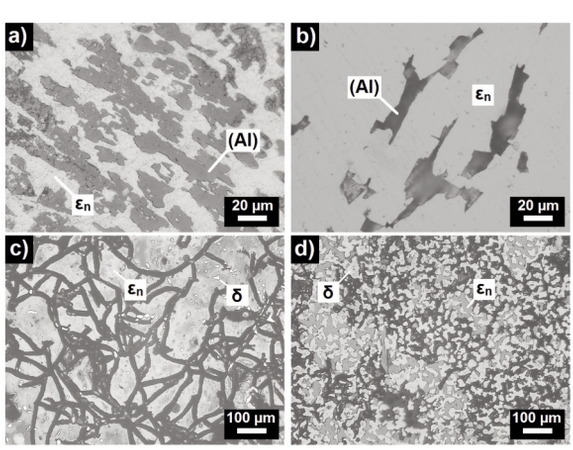

Figure 8. *Corroded surfaces of Al–Pd alloys after polarization in 0.01 M HCl: a) $Al_{88}Pd_{12}$, b) $Al_{77}Pd_{23}$, c) $Al_{72}Pd_{28}$, d) $Al_{67}Pd_{33}$.*

a preferential corrosion attack of ε_n has also been observed (Figs. 9c and 9d). The corrosion attack has been much more pronounced compared to the 0.01 M HCl solution. The electrochemical activity of phases in 0.01 M NaOH thus decreases in the following order:

$$(Al) < Al_3Pd\ (\varepsilon_n) < Al_3Pd_2\ (\delta) \quad (2)$$

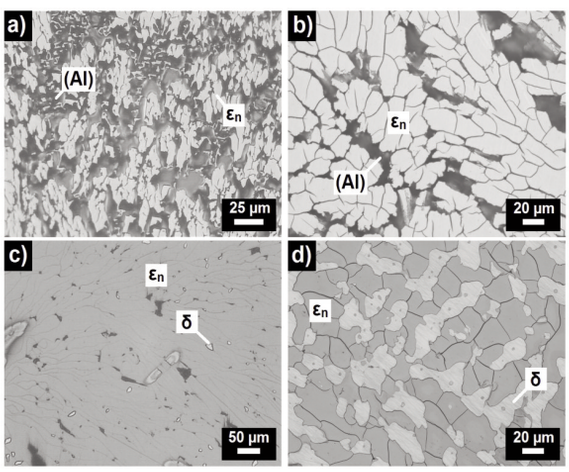

Figure 9. *Corroded surfaces of Al–Pd alloys after polarization in 0.01 M NaOH: a) $Al_{88}Pd_{12}$, b) $Al_{77}Pd_{23}$, c) $Al_{72}Pd_{28}$, d) $Al_{67}Pd_{33}$.*

Since Al alloys are prone to localized corrosion in Cl-containing electrolytes, the susceptibility of the Al–Pd alloys towards pitting in HCl has been further investigated by cyclic polarization. The cyclic polarization curves are presented in Fig. 10. For the alloys, a positive hysteresis loop has been found upon reverse polarization in 0.01 M HCl (Fig. 10). This observation is indicative of localized corrosion [32]. The physical origins behind the positive hysteresis lie in the connection between the critical crevice solution (CCS), the stability of pits, and the actual competition between diffusion and dissolution at localized corrosion sites [32]. During the initial portion of the reverse scan, the driving force for dissolution is decreasing, but CCS has not had sufficient time to diffuse away. As the reverse scan continues, the driving force for dissolution continues to decrease, and eventually the CCS cannot be maintained against diffusion. At this point, the localized corrosion sites re-passivate, and the anodic current drop is observed (Fig. 10). Throughout the scan, the areas on the surface that were not dissolving at high rate were having the passive films covering them thicken. Thus the re-passivation potential is a convolution of the loss of the CCS from the localized corrosion site and the raising of the corrosion potential of the surrounding passive surface (ennoblement) due to a decrease in anodic kinetics [32].

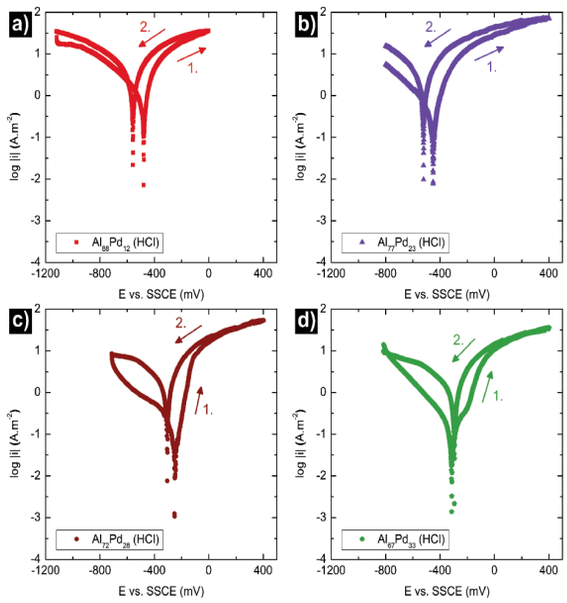

Figure 10. *Cyclic polarization curves of as-solidified Al–Pd alloys in 0.01 M HCl: a) $Al_{88}Pd_{12}$, b) $Al_{77}Pd_{23}$, c) $Al_{72}Pd_{28}$, d) $Al_{67}Pd_{33}$.*

For the Al–Pd alloys in 0.01 M NaOH, a negative loop occurs, i.e. the current densities on the reverse scan are smaller than those on the forward scan at the same potential (Fig. 11). On the reverse scan, the currents are lower at all potentials because of the thickened passive film. In these cases the pitting corrosion can be ruled out.

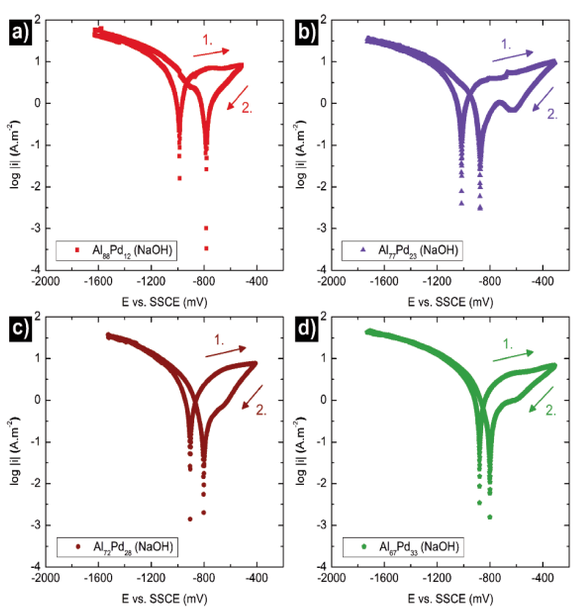

Figure 11. *Cyclic polarization curves of as-solidified Al–Pd alloys in 0.01 M NaOH: a) $Al_{88}Pd_{12}$, b) $Al_{77}Pd_{23}$, c) $Al_{72}Pd_{28}$, d) $Al_{67}Pd_{33}$.*

4. Conclusions

In the present work, both microstructure and corrosion performance of as-solidified alloys $Al_{88}Pd_{12}$, $Al_{77}Pd_{23}$, $Al_{72}Pd_{28}$ and $Al_{67}Pd_{33}$ (element concentrations are given in at.%) were investigated. The corrosion performance of the alloys was studied by potentiodynamic polarization in aqueous HCl and NaOH solutions at 21±2°C.

The alloys were found to consist of two single-phase microstructure constituents. Alloys $Al_{88}Pd_{12}$, $Al_{77}Pd_{23}$ were composed of (Al) and ε_n (ε_6+ε_{28}), and alloys $Al_{72}Pd_{28}$ and $Al_{67}Pd_{33}$ comprised ε_n (ε_6+ε_{28}) and δ. Alloys with the same phase constitution were found to have different volume fractions of constituents/phases. Each of the identified phases showed only negligible variations in metal composition across the set of investigated alloys.

The OCPs of the alloys increased with increasing Pd concentration. The corrosion parameters obtained by sample polarization were found to vary with both electrolyte and alloy bulk composition. Higher corrosion currents and lower corrosion potentials have been found for 0.01 M NaOH solution.

The susceptibility of the alloys towards localised corrosion was studied by cyclic polarization. In 0.01 M HCl a positive hysteresis was found, i.e., the current densities on the reverse scan were higher than those on the forward scan at the same potential. This result indicates a possible pitting behaviour of the materials in HCl solution.

Specific corrosion attack of different intermetallic phases was studied by investigating the alloy microstructure after electrode polarization. The electrochemical activity of phases in 0.01 M NaOH was found to decrease in the following order:

$$(Al) < Al_3Pd\ (\varepsilon_n) < Al_3Pd_2\ (\delta)$$

In 0.01 M HCl aqueous solution, a preferential dissolution of (Al) in alloys $Al_{88}Pd_{12}$ and $Al_{77}Pd_{23}$ has been found. The corrosion attack was, however, much less pronounced compared to the 0.01 M NaOH solution. This observation indicates that Al-Pd alloys are more susceptible to uniform (general) corrosion in basic solutions compared to acidic solutions.

A preferential corrosion attack of ε_n (Al_3Pd) has been found in alloys $Al_{72}Pd_{28}$ and $Al_{67}Pd_{33}$. The corrosion attack of this phase has resulted in a porous, channel-like framework. The inter-penetrating channels are probably a result of selective dissolution of Al from this phase (de-alloying). Further aspects of these interactions are currently under investigation and will be reported in a future publication.

Acknowledgements

This work was supported by the European Regional Development Fund (ERDF) project no. ITMS:26220120014 "Center for Development and Application of Advanced Diagnostic Methods in Processing of Metallic and Non-metallic Materials" funded within the Research & Development Operational Programme, the Grant Agency VEGA project nos. 1/0068/14, 1/0018/15 and 1/0465/15, and the Slovak Research and Development Agency project no. APVV-15-0049.

References

[1] J. M. Dubois, Chem. Soc. Rev., 41 (2012) 6760–6777.
[2] T. Duguet, S. Kenzari, V. Demange, Th. Belmonte, J. M. Dubois, V. Fournee, J. Mater. Res., 25 (2010) 764-772.
[3] M. Armbrüster, R. Schlögl, Y. Grin, Sci. Technol. Adv. Mater., 15 (2014) 034803.
[4] L. Soler, J. Macanás, M. Muñoza, J. Casado, Int. J. Hydrogen Energy, 32 (2007) 4702 – 4710.
[5] S. Kenzari, D. Bonina, J. M. Dubois, V. Fournée, Sci. Technol. Adv. Mater., 15 (2014) 024802.
[6] R. H. Estrada-Ruiz, R. Flores-Campos, G. A. Trevino-Rodrigues, J. M. Herrera-Ramirez, R. Martinez-Sanches, J. Min. Metall. Sect. B-Metall, 52 (2016), 163-170.
[7] B. Grushko, J. Alloy. Compd., 557 (2013) 102–111.
[8] L. Ďuriška, I. Černičková, R. Čička, J. Janovec, J. Phys. Conf. Ser., 809 (2017) 012008.
[9] A. Smontara, I. Smiljanić, A. Bilušić, B. Grushko, S. Balanetskyy, Z. Jagličić, S. Vrtnik, J. Dolinšek, J. Alloy. Compd., 450 (2008) 92–102.
[10] J. Hafner, M. Krajčí, Acc. Chem. Res., 47 (2014) 3378−3384.
[11] V. A. Drozdov, P. G. Tsyrulnikov, V. V. Popovskii, N. N. Bulgakov, E. M. Moroz, T. G. Galeev, React. Kinet. Catal. Lett., 27 (1985) 425–427.
[12] V. Johánek, I. Stará, V. Matolín, Surf. Sci. 507–510 (2002) 92–98.
[13] K. S. Chang, X. Peng, J. Indus. Eng. Chem., 16 (2010) 455–460.
[14] A. Lekatou, A. K. Sfikas, C. Petsa, A. E. Karantzalis, Metals, 6 (2016) 3.
[15] M. Palcut, P. Priputen, K. Šalgó, J. Janovec, Mater. Chem. Phys., 166 (2015) 95–104.
[16] M. Palcut, P. Priputen, M. Kusý, J. Janovec, Corros. Sci. 75 (2013) 461–466.
[17] A. Lekatou, A. K. Sfikas, A. E. Karantzalis, D. Sioulas, Corros. Sci. 63 (2012) 193–209.
[18] E. Huttunen–Saarivirta, T. Tiainen, Mater. Chem., Phys., 85 (2004) 383–395.
[19] Y. Massiani, S. Ait Yaazza, J. P. Crousier, J. M. Dubois, J. Non–Cryst. Solids, 159 (1993) 92–100.
[20] A. Rüdiger, U. Köster, J. Non–Cryst. Solids, 250–252 (1999) 898–902.
[21] A. Beni, N. Ott, E. Ura–Bińczyk, M. Rasinski, B. Bauer, P. Gille, A. Ulrich, P. Schmutz, Electrochim. Acta, 56 (2011) 10524–10532.
[22] E. Ura–Binczyk, N. Homazava, A. Ulrich, R. Hauert, M. Lewandowska, K. J. Kurzydlowski, Corros. Sci., 53

(2011) 1825–1837.

[23] P. Priputen, M. Palcut, M. Babinec, J. Mišík, I. Černičková, J. Janovec, J. Mater. Eng. Perform., 26 (2017) 3970-3976.

[24] Q. Zhang, Z. Zhang, Phys. Chem. Chem. Phys., 12 (2010) 1453–1472.

[25] J. Erlebacher, M. J. Aziz, A. Karma, N. Dimitrov, K. Sieradzki, Nature, 410 (2001) 450–453.

[26] Z. Zhang, Y. Wang, Z. Qi, W. Zhang, J. Qin, J. Frenzel, J. Phys. Chem. C 113 (2009) 12629–12636.

[27] X. Wang, W. Wang, Z. Qi, C. Zhao, H. Ji, Z. Zhang, Electrochem. Commun. 11 (2009) 1896–1899.

[28] J. Zhang, M. Klasky, B. C. Letellier, J. Nuclear Mater., 384 (2009) 175–189.

[29] M. Christopher, A. Brett, Corros. Sci, 33 (1992) 203-210.

[30] B. N. Popov, Corrosion Engineering Principles and Solved Problems, Elsevier, New York, 2015, pp. 29–92.

[31] E. McCafferty, Introduction to Corrosion Science, Chapter 6 Thermodynamics of Corrosion: Pourbaix Diagrams, Springer Science+Business Media, LLC 2010.

[32] R. G. Kelly, J. R. Scully, D. W. Shoesmith, R. G. Buchheit, Electrochemical Techniques in Corrosion Science and Engineering, Marcel Dekker, New York, 2003, pp. 29–92.